ACS OMEGA

Open Access

http://pubs.acs.org/journal/acsodf

Article

Enhanced Gas Barrier and Mechanical Properties of Styrene−Butadiene Rubber Composites by Incorporating Electrostatic Self-Assembled Graphene Oxide @ Layered Double Hydroxide Hybrids

Xi Zhang, Zongchao Xu, Chongzhi Sun, Long Zheng,* and Shipeng Wen*

Cite This: *ACS Omega* 2024, 9, 39846−39855

Read Online

ACCESS | Metrics & More | Article Recommendations

ABSTRACT: Rubber composites with a high gas barrier and mechanical properties have received considerable attention due to their potential applications. Constructing complex filler networks in a rubber matrix is an effective strategy to simultaneously enhance the gas barrier and mechanical properties. In this work, graphene oxide layered double hydroxide (GO@LDHs) hybrids were obtained by the electrostatic self-assembly method. A unique interspersed and isolated structure was formed in GO@LDHs hybrids due to the chemical interactions between the functional groups on GO sheets and the metal cations on LDH layers. Subsequently, the GO@LDHs hybrids were incorporated into a styrene−butadiene rubber (SBR) matrix using a green latex compounding method. The results showed that the GO@LDHs hybrids were uniformly embedded in the SBR matrix, constructing an overlapped filler network and forming physical bonding points that reduced the free volume of the composites. The electrostatic interactions between GO@LDHs hybrids facilitated energy dissipation during stretching, thereby improving the mechanical performance of the rubber composites. More importantly, the N_2 gas permeability and fracture toughness of GO@LDHs/SBR composites decreased by 52.2% and increased by 845%, respectively, compared to those of a pure SBR matrix. The construction of GO@LDHs hybrids offers new insights for designing rubber composites with a high gas barrier and mechanical properties.

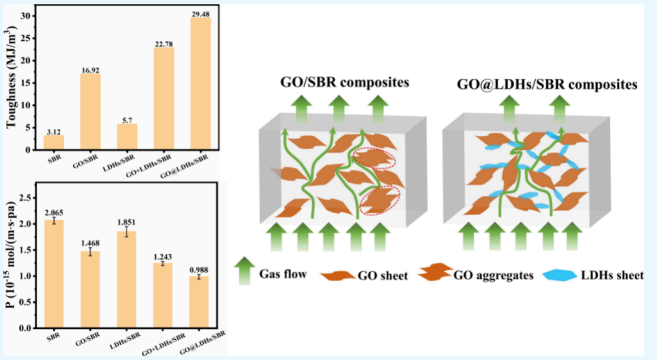

1. INTRODUCTION

Rubber composites with high barrier properties are essential in industries dealing with gas or liquid containment, such as tire inner tubes, seal rings, and air springs.[1,2] Their high elasticity and ability to recover from deformation make them indispensable in these applications. In the case of tires, effective gas barrier properties are crucial for minimizing abrasion, reducing rolling resistance, and ensuring overall driving safety. Poor gas barrier properties lead to a gradual loss of inflation pressure during tire service, resulting in increased tire wear and rolling resistance.[3] Studies indicated that rolling resistance increased by 2.5% per 10 kPa loss in inflation pressure, thus elevating vehicle energy consumption.[4] Therefore, the urgent development of rubber composites with tailored superior gas barrier properties for tires is crucial, not only for energy savings but also for environmental protection. Meanwhile, considering the high cost of butyl rubber with excellent barrier properties, it is of great significance to develop high gas barrier rubber composites based on general-purpose rubbers such as styrene−butadiene rubber (SBR).

Generally, most rubber matrices possess poor gas barrier properties owing to the substantial free volumes present among rubber molecular chains. Various strategies, including heterogeneous cross-linking,[5] layer-by-layer assembly,[6] and incorporation of impermeable two-dimensional (2D) layered fillers (e.g., layered silicate,[7] graphene,[8] boron nitride,[9] etc.) have been employed to enhance the barrier properties of rubber composites. Among these methods, the incorporation of impermeable layered fillers is a simple and effective method of tailoring the barrier properties of rubber composites. The layered fillers construct a tortuous diffusion path that prevents the gas molecule diffusion; meanwhile, the interface between the layered fillers and rubber matrix constrains the mobility of

Received: June 5, 2024
Revised: August 28, 2024
Accepted: September 5, 2024
Published: September 10, 2024

rubber molecular chains, consequently reducing the free volumes and lowering gas permeability. Graphene oxide (GO), characterized by a large specific surface area and high aspect ratio, emerges as an ideal candidate for a barrier-layered filler in a rubber matrix. For example, Razzaghi-Kashani et al. demonstrated a 45% reduction in N_2 permeability in GO/styrene−butadiene rubber (GO/SBR) with 4 parts per hundreds of rubber (phr) GO prepared via latex compounding.[10] Zheng et al. observed a 46% decrease in the diffusion coefficient of sulfur mustard in GO/butyl rubber composites with 3 phr GO content.[11] Yang et al. showed a 69% improvement in the gas barrier property by introducing 3 phr amphiphilic GO cross-linkers (R-aGO) into brominated butyl rubber (BIIR).[12] Zhang et al. observed that GO as a barrier additive achieved 80% reduction in ammonia permeability reduction of nitrile-butadiene rubber (NBR), although this also resulted in a more rigid elastomer.[13] Nevertheless, achieving low gas permeability necessitates a relatively high mass loading of GO, leading to GO aggregation and subsequently compromising the mechanical toughness of the rubber composites. In previous studies, it was found that the filler network is crucial for enhancing the gas barrier performance of rubber composites. As the amount of graphene or GO increases, the gas permeability gradually decreases. However, the GO layer structure exhibits a strong adsorption effect on rubber molecular chains, which can lead to improved gas barrier performance at the expense of the elongation at break. For example, Wang et al. reported that with a 3 wt % GO content, the gas permeability was reduced to 44% of that of pure rubber, while the elongation at break decreased by approximately 33%.[14] Therefore, it is essential to balance the enhancement of the gas barrier performance with the preservation of mechanical strength and elongation properties in rubber composites.

In recent years, decorating nanoparticles (e.g., silica, carbon black, zinc oxide, carbon nanotubes, etc.) on GO sheets has emerged as an effective strategy to enhance the dispersion of GO. These hybridized fillers prevent the restacking of GO sheets and the aggregation of other fillers, thus exhibiting a superior synergistic effect on the barrier performance. Moreover, the hybridized filler network preferentially breaks upon deformation due to the lower bond energy between fillers compared to the C−C covalent bonds of the rubber molecules.[15] Previous studies by Liu et al. showcased the development of graphene nanosheets decorated with ZnO nanoparticles, resulting in rubber composites with enhanced mechanical and gas barrier properties.[16]

Layered double hydroxide (LDH) is a typical class of 2D ionic layered materials consisting of positively charged layers and charge-balancing anions situated between the hydrotalcite layers.[17] Previous research has extensively employed LDHs in polymer packaging films (e.g., polyethylene terephthalate, poly(vinyl alcohol), polylactic acid, etc.), attributing to the ability to enhance both gas barrier properties and mechanical properties of polymer composites.[18−20] Dou et al. investigated the strong adsorption capabilities of LDHs for CO_2 molecules, whereby the chemically adsorbed CO_2 occupied free volume at the filler/polymer interface, consequently reducing the diffusion of oxygen molecules.[21] Yang et al. fabricated a hybrid film that sodium dodecyl sulfate (SDS)-modified LDH integrated with poly(butylene adipate-terephthalate) (PBAT) matrix, and the optimized SDS@LDH (5%)/PBAT composite film showed that the water vapor transmission rates (WVTR) and oxygen transmission rates (OTR) improved ∼72% and ∼52% compared with pure PBAT film.[22] Li et al. developed a modified Ca−Mg−Al LDH into silicone rubber (SR), and due to the homogeneous dispersion and good compatibility, SR/modified LDH nanocomposites showed satisfactory mechanical properties and improved gas barrier properties.[23] However, limited attention has been given to exploring the gas barrier properties of LDHs/rubber composites. Considering the unique structure and surface charge characteristics of GO and LDHs, preparing GO@LDHs hybrids holds significant promise for advancing applications in rubber composites.

In this research, GO@LDHs hybrids were prepared by the electrostatic self-assembly method. The dispersion stability, microstructure, and chemical composition of the GO@LDHs hybrids were analyzed. Subsequently, the GO@LDHs hybrids were incorporated into the SBR matrix using the latex coagulation method to produce GO@LDHs/SBR composites. The dispersion of GO@LDHs, filler network structure, dynamic and static mechanical properties, and gas barrier properties of the resulting SBR composites were then investigated.

2. EXPERIMENTAL SECTION

2.1. Materials. GO was prepared by a modified Hummers method.[24] LDHs were prepared by the SNAS method.[25] Styrene−butadiene rubber latex (SBR 1502, with a solid content of 20%) was provided by the Qilu Petrochemical Company. Zinc oxide, stearic acid, antioxidant 4020, antioxidant RD, accelerant CZ, and sulfur were all commercial products.

2.2. Preparation of GO@LDHs Hybrids. GO@LDHs hybrids were prepared by the electrostatic self-assembly method. Initially, GO aqueous dispersion with a concentration of 3 mg/mL and LDHs aqueous dispersion with a concentration of 10 mg/mL was prepared with ultrasonic equipment. Subsequently, the GO dispersion was transferred into a three-neck flask with continuous stirring at 50 °C. Then, the LDH dispersion was slowly dropped into the GO dispersion via a constant pressure funnel. The resulting mixture dispersion was stirred and homogenized at 50 °C for 1 h to yield a uniform GO@LDHs aqueous dispersion. Four distinct GO@LDHs hybrids were prepared with different GO/LDH mass ratios (1/0.5, 1/1, 1/3, and 1/5).

2.3. Preparation of GO@LDHs/SBR Composites. GO@LDHs/SBR composites were fabricated by a latex coagulation method. Specifically, a designed amount of GO@LDHs (1/3) aqueous dispersion was added to SBR latex under mechanical stirring for 30 min. The mixture was then coagulated using calcium chloride (1 wt %) solution. The obtained compounds were washed with enough deionized water and dried at 50 °C. Subsequently, the dried compounds were blended with the residual ingredients (as outlined in Table 1) on a two-roll mill and cured at 150 °C for an optimum cure time to obtain the final GO@LDHs/SBR composites. For comparison, GO/SBR, LDHs/SBR, and GO+LDHs/SBR (GO and LDHs were separately incorporated into SBR) composites were prepared by using the same procedure as mentioned above.

2.4. Characterization. The morphology of GO, LDHs, and GO@LDHs was observed on scanning electron microscopy (SEM, S4800, Hitachi). The samples were fractured in liquid nitrogen and then sprayed with gold before measurements. Elemental analysis was carried out on X-ray photoelectron spectroscopy (XPS, Escalab 250, Thermo Electron Corporation). The Fourier transform infrared spectra (FTIR) were conducted using an FTIR Spectrometer (Tensor 27, Bruker) in transmission mode with a scanning range from 4000 to 400 cm^{-1}

https://doi.org/10.1021/acsomega.4c05304
ACS Omega 2024, 9, 39846−39855

Table 1. Formula of SBR, GO/SBR, LDHs/SBR, GO+LDHs/SBR, and GO@LDHs/SBR Composites (the Unit is phr)

sample	SBR	GO/SBR	LDHs/SBR	GO+LDHs/SBR	GO@LDHs/SBR
SBR	100	100	100	100	100
GO	0	3	0	3	0
LDHs	0	0	9	9	0
GO@LDHs	0	0	0	0	12
stearic acid	1	1	1	1	1
zinc oxide	3.5	3.5	3.5	3.5	3.5
antioxidant 4020	2	2	2	2	2
antioxidant RD	2	2	2	2	2
accelerant CZ	2.2	2.2	2.2	2.2	2.2
sulfur	1.4	1.4	1.4	1.4	1.4

at room temperature. The resolution was set at 4 cm^{-1}, and each spectrum was scanned 32 times. X-ray diffraction (XRD) analysis was performed using an Ultima IV diffractometer (Rigaku, Japan) with Cu−Kα radiation (λ = 0.1542 nm) in the region of 5−60° at a scan rate of 5°/min at 40 kV. The zeta potential of GO, LDHs, and GO@LDHs dispersion was measured by a Malvern Zetasizer (Nano ZS, USA).

The filler network was assessed using a rubber processing analyzer (RPA2000, Alpha Technologies, USA) at 60 °C and 1 Hz. The GO@LDHs dispersion in SBR composites was observed by transmission electron microscopy (TEM, H-9500, Hitachi). The samples for TEM were prepared by cryo-ultramicrotomy, and the ultrathin sections with a thickness of around 50 nm were placed on a 300 mesh copper grid for observation. Mechanical properties were evaluated by using a tensile test machine (SANS, CTM4104, China). Tensile and tear properties were determined according to ISO 37:2017 and ISO 34−1:2022 standards, respectively. Young's modulus was calculated from the slope of the tensile curve in the linear region.[26] Shore A hardness was performed following ISO 868:2015. Dynamic mechanical properties of SBR composites were investigated on a dynamic mechanical thermal analyzer (DMTA, VA3000, Metravib) in tension mode with a heating rate of 3 °C/min and a frequency of 10 Hz. Nitrogen permeability tests were carried out on gas permeability-measuring equipment (VAC-V2, Labthink, China) according to ISO 2782−1:2022 standard. The samples used were circular specimens with a thickness of approximately 1 mm and diameter of 80 mm.

3. RESULTS AND DISCUSSION

3.1. The Dispersion and Morphology of GO@LDHs Hybrids. GO features abundant oxygen-containing groups, such as epoxy, hydroxyl, and carboxyl groups. Among them, carboxylic acid and phenolic hydroxyl groups ionized in water,[27] resulting in negatively charged surfaces of GO sheets, with a measured zeta potential of −51.3 mV (Figure 1b). Typically, an absolute value of the zeta potential exceeding 30 mV is considered indicative of stable dispersions owing to interparticle electrostatic repulsion.[28,29] Therefore, GO could stably disperse in water for over 7 days (Figure 1a) due to the electrostatic repulsion between sheets. Conversely, LDH layers exhibited a positive charge with a zeta potential of +15.6 mV (Figure 1b), attributing to the replacement of trivalent metal ions on the layer with divalent metal ions.[30] After the mixture was left to stand for 7 days, sedimentation occurred in its dispersion (Figure 1a). Based on the opposite charge characteristics of GO and LDHs, they readily underwent electrostatic self-assembly to form GO@LDHs hybrids. When the mass ratio of GO/LDHs increased from 1/0.5 to 1/3, GO@LDHs could stably disperse in water for over 7 days (Figure 1a), as their zeta potential values were all below −30 mV (Figure 1b). However, when the mass ratio of GO/LDHs reached 1/5, its zeta potential was −24.9 mV, indicating that the dispersion was unstable according to the criterion of colloidal stability,[27] which was also confirmed by the digital photograph in Figure 1a.

The morphologies of LDHs, GO, and GO@LDHs hybrids were characterized by SEM. In Figure 2a, LDHs exhibited irregular lamellar morphologies with dimensions ranging from hundreds of nanometers to several microns. However, several LDH layers were observed stacked together, forming aggregates (marked by red arrows). In Figure 2b, GO exhibited a thin and wrinkled layer structure, owing to the van der Waals force between GO sheets.[31] Figure 2c−f depicts the transition of GO@LDHs hybrids from densely folded lamellae to loosely lamellar structure with the increase of LDH content. This transition occurred because LDHs adsorbed on the surface of GO sheets prevented the self-aggregation of GO sheets. At high LDHs content, the negatively charged GO sheets adsorbed on positively charged LDHs, leading to excess LDHs forming aggregates. Therefore, the LDH content in the GO@LDHs hybrids has an optimal value, which was consistent with the observed morphology and measured zeta potential.

3.2. Chemical Structure Characterization of GO@LDHs Hybrids. FTIR spectra of GO, LDHs and GO@LDHs are shown in Figure 3a. For GO, the absorption peaks at 3417, 1739,

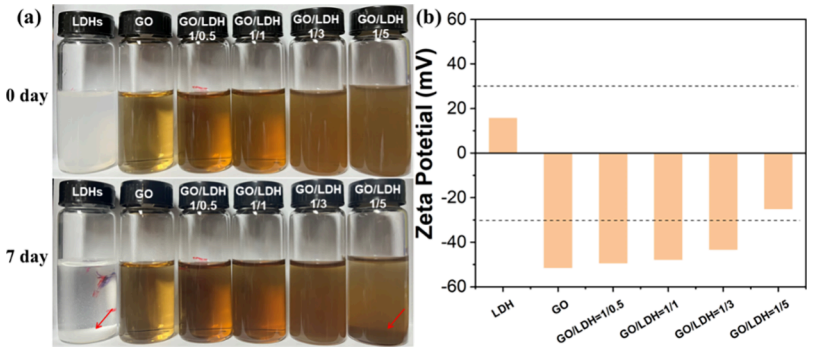

Figure 1. (a) Digital photographs of LDHs, GO, and GO@LDHs dispersions before and after storage for 7 days; (b) zeta potential of LDHs, GO, and GO@LDHs dispersions (pH = 8).

https://doi.org/10.1021/acsomega.4c05304
ACS Omega 2024, 9, 39846−39855

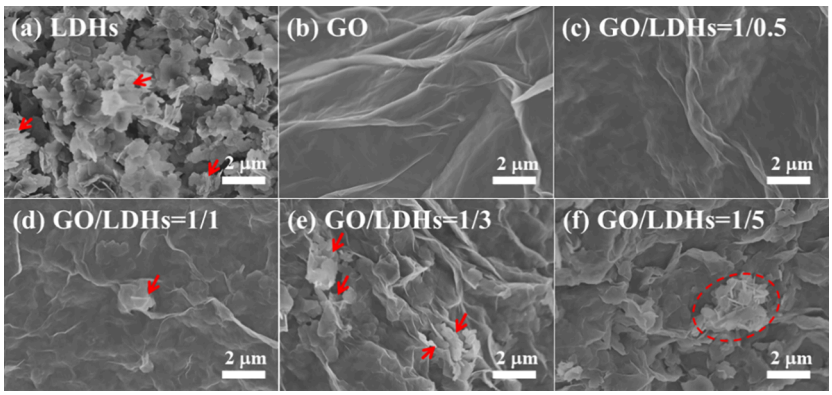

Figure 2. SEM images of (a) LDHs, (b) GO, and (c–f) GO@LDHs hybrids with different GO/LDHs mass ratios.

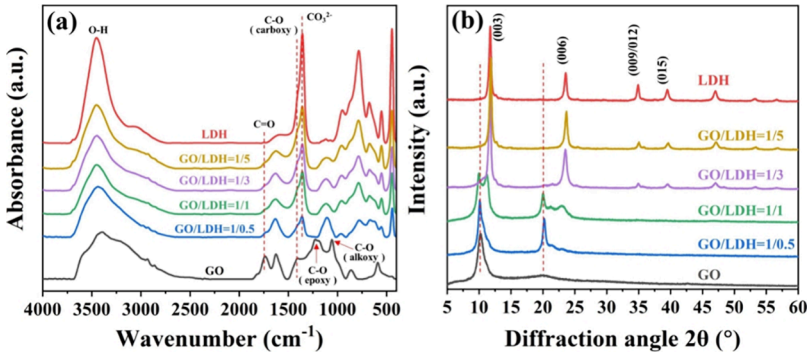

Figure 3. (a) FTIR and (b) XRD spectra of GO, LDHs, and GO@LDHs hybrids.

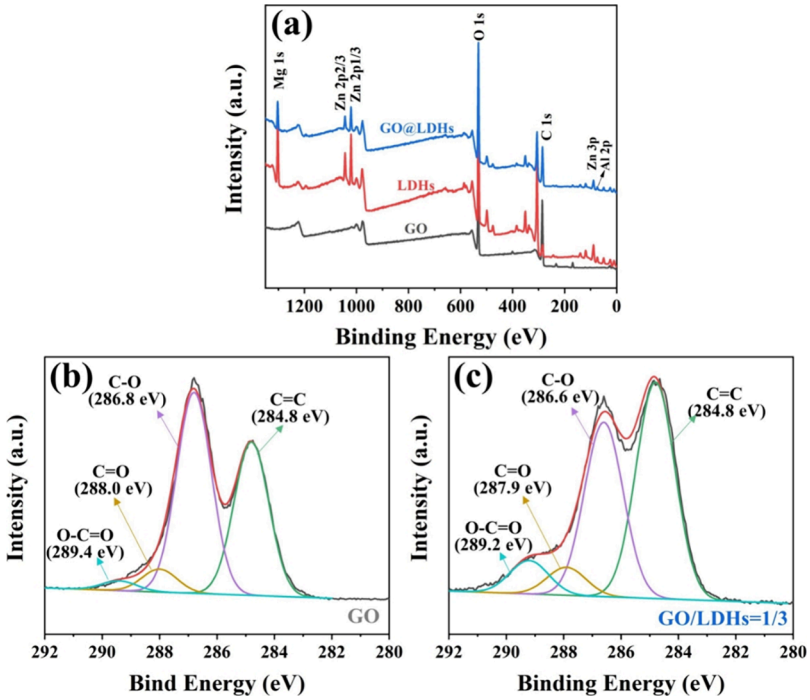

Figure 4. (a) XPS wide scan spectra of GO, LDHs and GO@LDHs hybrids (GO/LDHs = 1/3), (b) C 1s spectra of GO, and (c) C 1s spectra of GO@LDHs (GO/LDHs = 1/3).

1627, 1408, 1230, and 1057 cm^{-1} originated from the stretching vibration of O−H, C═O, C═C of the aromatic ring, C−O in carboxy, C−O in epoxy, and C−O in alkoxy, respectively.[32,33] For LDHs, the peaks at 3454 and 1610 cm^{-1} were assigned to the stretching vibration of O−H groups and the deformation vibration of interlayer water molecules.[34] Additionally, the sharp peak at 1357 cm^{-1} was attributed to the stretching vibration of the CO_3^{2-} groups between the LDHs layers,[35] while the peaks in the 500−1000 cm^{-1} range were assigned to the vibration of M−O, M−OH, and O−M−O in the LDHs lattice (M = Mg, Al,

https://doi.org/10.1021/acsomega.4c05304
ACS Omega 2024, 9, 39846−39855

Zn).[36] Comparatively, in GO@LDHs, the stretching vibration of C═O at 1739 cm^{-1} gradually disappeared with the increase of LDHs content, whereas the peak related to carboxy C−O vibration at 1408 cm^{-1} shifted to a low wavenumber. This alteration was attributed to the chelation between the negatively charged $-COO^-$ located on the edge of GO sheets and the positively charged LDH sheets.[37] Furthermore, the peak of epoxy C−O at 1230 cm^{-1} nearly disappeared in GO@LDHs hybrids, while a new type of C−O bonds at 1107 cm^{-1} emerged, induced by the ring-opened reactive epoxy groups in GO sheets in the presence of metal cations in the LDHs lattice.[38,39]

The crystal structure of GO, LDHs, and GO@LDHs hybrids was investigated by XRD analysis. As shown in Figure 3b, the GO curve showed a prominent diffraction peak at $2\theta = 10.2°$, indicating an interlayer spacing of 0.866 nm according to the Bragg law.[40] Meanwhile, the LDH curve displayed typical diffraction peaks (003), (006), (009), and (015), consistent with the previous study.[41] Notably, in GO@LDHs hybrids, a unique layer stacking structure emerged between GO and LDHs. Specifically, when the GO/LDHs mass ratio was 1/0.5 and 1/1, the characteristic diffraction peak of GO and the typical diffraction peaks (003), (006) of LDHs shifted to lower 2θ values, suggesting an increased interlayer space of both GO and LDHs. With increasing LDH content, the characteristic diffraction peak of GO gradually disappeared owing to the intercalation of the GO layers by LDH sheets. The XRD analysis revealed the interspersion of GO and LDH layers, forming newly assembled GO@LDHs hybrids, which effectively hindered the aggregation of the GO sheets.

XPS was performed to investigate the chemical composition of GO, LDHs, and GO@LDHs hybrids. Figure 4a shows the survey spectra of GO@LDHs hybrids, revealing the presence of C, O, Al, Zn, and Mg elements derived from GO and LDHs. Figure 4b,c compares the C 1s spectra of GO and GO@LDHs hybrids. In the spectrum of GO, peaks at 284.8, 286.8, 288.0, and 289.4 eV were assigned to C═C, C−O, C═O, and O−C═O functional groups, respectively.[42] In contrast, the C−O peak in the spectrum of GO@LDHs hybrids shifted to lower binding energy with decreased intensity, indicating the formation of hydroxyl groups (C−OH) resulting from the ring-opening of the reactive epoxy groups in GO sheets induced by the metal cations in LDHs lattice.[37,43,44] Subsequently, the metal cations in LDH layers formed coordinate-covalent bonds or alkoxides with hydroxyl groups.[37] Meanwhile, the peak corresponding to O−C═O groups shifted slightly from 289.4 to 289.2 eV, suggesting the formation of metal-carboxylate chelates between the metal cations of LDHs and carboxylic acid groups of GO.[38]

Based on the above analysis, there are two types of interactions between LDHs and GO sheets, as illustrated in Figure 5. One involves the interlayer interaction between the metal cations on LDH layers and hydroxyl groups on GO basal planes. The other involves the bridging bonding between metal cations on the LDH layers and carboxylic acid groups at the edge of GO sheets. The strong interactions between GO and LDHs resulted in a unique lamellar interspersed isolation structure, effectively preventing the aggregation of GO and LDHs. However, the ratio of GO and LDHs also affected the lamellar assembled structure. In the GO@LDHs (GO/LDHs = 1/3) aqueous dispersion, no apparent aggregation was observed, and it remained stably dispersed. Therefore, GO@LDHs (GO/LDHs = 1/3) hybrids were selected for further application studies in rubber composites.

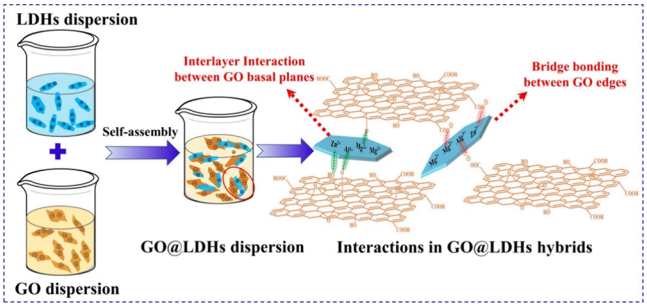

Figure 5. Schematic preparation and interaction model of GO@LDHs.

3.3. Dispersion State of GO@LDHs Hybrids in SBR Composites. To ensure the dispersion of lamellar filler in the rubber matrix, the green latex coagulation method was used to fabricate the SBR composites.[45] TEM measurements were conducted to evaluate the dispersion state of the fillers in the SBR matrix. In the TEM images of Figure 6, the bright area mainly represented the SBR matrix, while the dark line and sheets represented the lamellar fillers. As shown in Figure 6a,a′, GO exhibited uneven dispersion, and local aggregation was observed, forming black aggregates with sizes ranging from 200 to 300 nm (marked by the red arrows). For LDHs/SBR composites in Figure 6b,b′, the dark lines represented incorporated LDH layers, indicating the formation of severe large aggregates with sizes ranging from 200 to 400 nm. In Figure 6c,c′, GO+LDHs/SBR composites exhibited apparent stacking of layers due to the direct addition of GO and LDHs, indicating the interaction forces between layers cannot be overcome and the aggregates formed by the layers stacking (marked by the red arrows). However, in Figure 6d&d′, GO@LDHs/SBR composites exhibited uniform dispersion throughout the SBR matrix without large aggregations. Many thin individual GO sheets were isolated by LDH layers, suggesting that the GO@LDHs hybrids easily achieved synergistic dispersion in the SBR matrix.

3.4. Filler Network of GO@LDHs Hybrids in SBR Composites. The filler network within rubber composites is essential to prolong the diffusion path of gas molecules and improve the gas barrier performance.[14,46] The filler network was evaluated by an RPA2000. As shown in Figure 7, the storage modulus (G') of all SBR composites decreased with increasing strain amplitude, owing to the "Payne effect" caused by the breakdown of the filler network and release of the trapped rubber under oscillatory shear force.[47,48] Compared with the pure SBR, the addition of layered fillers resulted in an increase in G' of the SBR composite. The G' of GO/SBR composites was higher than that of LDHs/SBR composites, which indicated that GO with a high specific surface area formed more physical bonding points with the SBR matrix compared to LDHs. When added in equal proportion, the G' of GO@LDHs/SBR was significantly higher than that of GO+LDHs/SBR composites. This enhancement was attributed to the uniform dispersion of GO@LDHs hybrids, which facilitated the formation of an overlapped filler network and physical bonding points. Additionally, from the TEM images in Figure 6d,d′, it can be inferred that the GO@LDHs/SBR composites formed a tortuous filler network, thereby prolonging the penetration path of gas molecules and improving the gas barrier performance of the SBR composites.

It is still challenging to develop rubber composites with high tensile strength and large elongation at break. Figure 8a presents

https://doi.org/10.1021/acsomega.4c05304
ACS Omega 2024, 9, 39846−39855

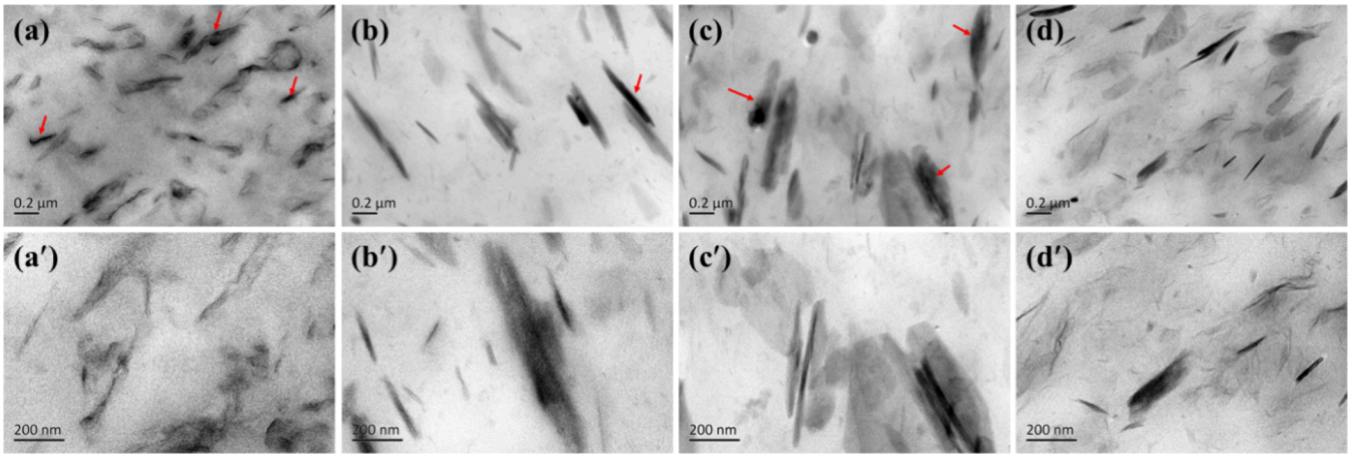

Figure 6. TEM images of (a,a′) GO/SBR, (b,b′) LDHs/SBR, (c,c′) GO+LDHs/SBR, and (d,d′) GO@LDHs/SBR composites.

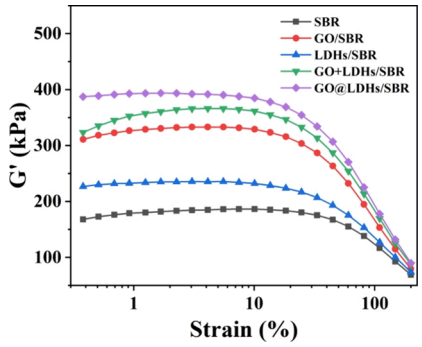

Figure 7. Storage modulus vs dynamical strain amplitude curves of SBR composites.

the stress−strain curves of all SBR composites, and the data on mechanical properties are listed in Table 2. The pure SBR matrix exhibited a relatively low tensile strength and elongation at break. Upon incorporation of GO or/and LDHs into SBR matrix, the tensile strength of GO/SBR and LDHs/SBR surpassed that of the pure SBR matrix. Compared with GO/SBR, LDHs/SBR, and GO+LDHs/SBR composites, the tensile strength of GO@LDHs/SBR composites increased 61.0%, 407.7%, and 36.1%, respectively. Notably, the elongation at break of GO@LDHs/SBR was also higher than that of GO/SBR, LDHs/SBR, and GO+LDHs/SBR composites. Meanwhile, GO@LDHs/SBR also possessed the highest hardness, Young's modulus, and tear strength. The concurrent improvement in tensile strength and elongation at break for GO@LDHs/SBR composites was considered significant, as indicated by the calculated fracture toughness in Figure 8b, which was defined as the area under the stress−strain curve.

Generally, the dispersion of fillers and the interfacial interaction between fillers and the rubber matrix were crucial factors in tailoring the mechanical properties of rubber composites. The desirable performance of GO@LDHs/SBR composites was ascribed to two reasons: (1) the GO@LDHs hybrids improved the dispersion of GO and LDHs sheets in SBR matrix and forming a strong interfacial interaction with SBR matrix, thereby restricting molecular chain slip and increasing the tensile stress; (2) the electrostatic interaction in GO@LDHs hybrids preferentially broke upon deformation, which provided sacrificial bonds that dissipate energy, resulting in high tensile strength and elongation.[15]

3.5. Dynamic Mechanical Properties of SBR Composites. The interfacial interactions between fillers and the SBR matrix were further investigated by DMA. The storage modulus (E') and loss factor (tan δ) versus temperature curves of all SBR composites are presented in Figure 9. It is evident from Figure 9a that the E' of GO@LDHs/SBR composites was higher than that of GO/SBR, LDHs/SBR, and GO+LDHs/SBR composites, indicating that the incorporation of GO@LDHs hybrids into the SBR matrix significantly improved the stiffness of SBR composites due to the large specific area and ultrahigh modulus of GO@LDHs hybrids. Generally, the temperature corresponding to the peak value of the loss factor curve is identified as glass transition temperature (Tg). As shown in Figure 8b, after adding the lamellar filler, the position of the peak of tan δ did not change

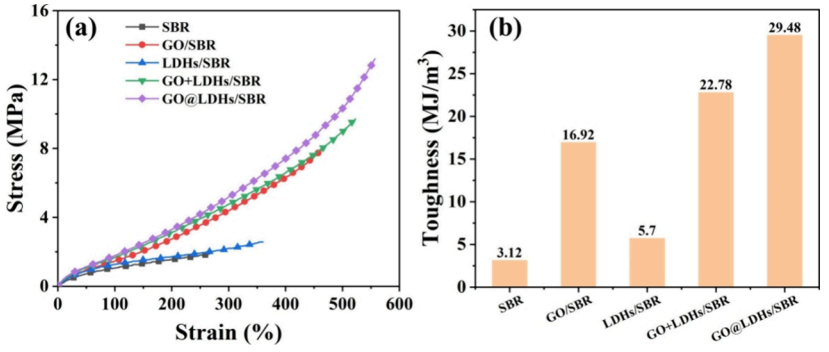

Figure 8. (a) Stress−strain curves and (b) fracture toughness of all SBR composites.

https://doi.org/10.1021/acsomega.4c05304
ACS Omega 2024, 9, 39846−39855

Table 2. Mechanical Properties of All SBR Composites

samples	hardness (shore A)	Young's modulus (MPa)	modulus at 100% elongation (MPa)	modulus at 300% elongation (MPa)	tensile strength (MPa)	elongation at break (%)	tear strength (kN/m)
SBR	47 ± 1	2.3 ± 0.1	1.0 ± 0.1		1.9 ± 0.1	267 ± 8	9.5 ± 0.9
GO/SBR	51 ± 1	3.7 ± 0.1	1.5 ± 0.1	4.4 ± 0.1	8.2 ± 0.1	471 ± 12	20.8 ± 1.2
LDHs/SBR	50 ± 1	2.9 ± 0.1	1.3 ± 0.1	2.2 ± 0.1	2.6 ± 0.1	360 ± 10	10.8 ± 1.0
GO+LDHs/SBR	52 ± 1	4.2 ± 0.1	1.7 ± 0.1	4.8 ± 0.1	9.7 ± 0.3	523 ± 12	23.8 ± 1.3
GO@LDHs/SBR	53 ± 1	4.8 ± 0.1	1.8 ± 0.1	5.2 ± 0.1	13.2 ± 0.4	557 ± 11	28.9 ± 1.5

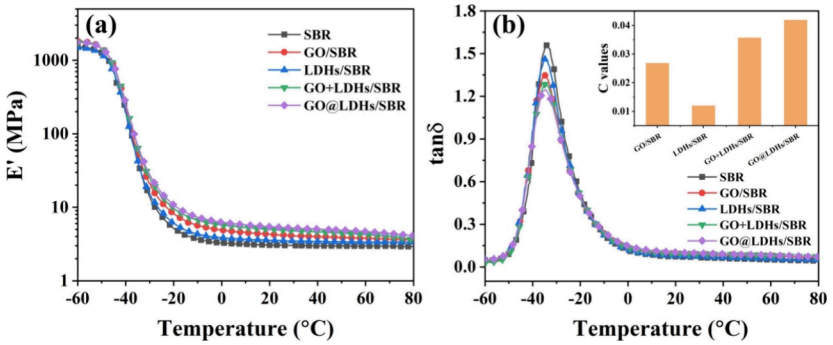

Figure 9. (a) Storage modulus versus temperature and (b) loss factor versus temperature curves of all SBR composites; the inset is the C values of the composites.

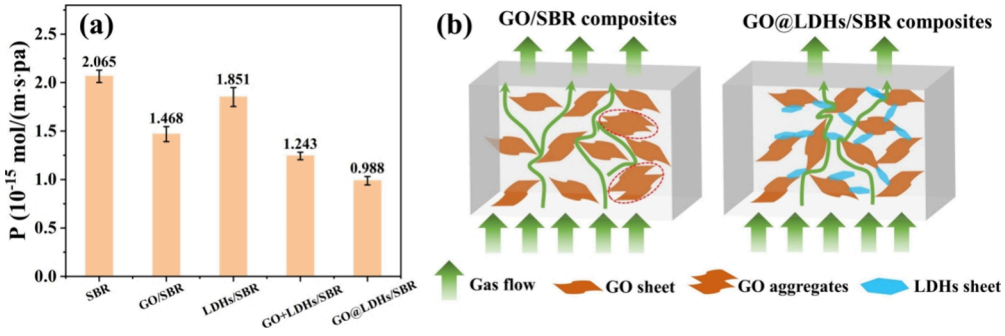

Figure 10. (a) N_2 gas permeability of all SBR composites and (b) the diagram of the gas flow diffusion in GO/SBR and GO@LDHs/SBR composites.

significantly, which is consistent with the previous research.[49] However, the height of the tan δ peak decreased notably, indicating that the filler adsorbed the SBR molecular chain and reduced the content of polymer that can participate in the movement of chain segments. To understand the effect of constrained polymer on dynamical mechanical properties, the fraction of restricted SBR chains region (C) can be calculated by the following equation[50,51]

$$C = 1 - \frac{(1 - C_0)B}{B_0}$$

where the C_0 and B_0 are the fraction of restricted regions and the fraction of energy loss in the pure SBR matrix, respectively. Here, C_0 is taken as 0. The fraction of energy loss of filled SBR composites can be determined by the following equation:

$$B = \frac{\pi \tan\delta}{\pi \tan\delta + 1}$$

Through calculations, the results are shown in the inset of Figure 9b. The C value of GO@LDHs/SBR composites was higher than that of GO/SBR, LDHs/SBR, and GO+LDHs/SBR composites, suggesting that the stronger interfacial interaction between GO@LDHs hybrids and the SBR matrix, leading to more volume of constrained SBR molecular chains. Therefore, it can be further concluded that the constrained regions reveal a positive effect on the mechanical performances of the composites.

3.6. Gas Barrier Properties of SBR Composites. The gas barrier properties of SBR composites filled with different fillers are presented in Figure 10. For the pure SBR matrix, the N_2 permeability was relatively high due to the large free volumes between the rubber molecules. For GO/SBR composites, the N_2 permeability decreased by 28.9% compared to that of the pure SBR matrix owing to the formation of the gas barrier filler network by GO layers. The N_2 permeability of LDHs/SBR composites was much higher than that of GO/SBR composites due to the low specific surface area and aggregation of LDHs sheets. Compared with GO/SBR, LDHs/SBR, and GO+LDHs/SBR composites, the N_2 permeability of GO@LDHs/SBR was decreased by 32.7%, 46.6%, and 20.5%, respectively. The gas flow diffusion diagrams in GO/SBR and GO@LDHs/SBR composites are displayed in Figure 9b. For GO@LDHs/SBR composites, the significant improvement in gas barrier properties can be attributed to two main reasons. First, GO and LDHs are interspersed to form an isolated and dispersed layer

https://doi.org/10.1021/acsomega.4c05304
ACS Omega 2024, 9, 39846−39855

structure, and the overlapped layer creates a complex gas barrier network, prolonging the pathways of N_2 in the SBR matrix. Second, a stronger interfacial interaction was formed between the homogeneously dispersed GO@LDHs hybrids and SBR matrix, which restricted more molecular movement of the SBR matrix and thus reduced the free volume of the composites.[52] Therefore, the experimental results also prove that GO@LDHs exhibit excellent characteristics to improve the gas barrier performance of rubber composites. Comparisons of tensile strength, elongation at break, and reduction in permeability of the composites between this work and other previously published works[53−57] are summarized in Figure 11. GO@LDHs/SBR composites exhibited a comprehensive advantage in the improvement of both mechanical and barrier properties.

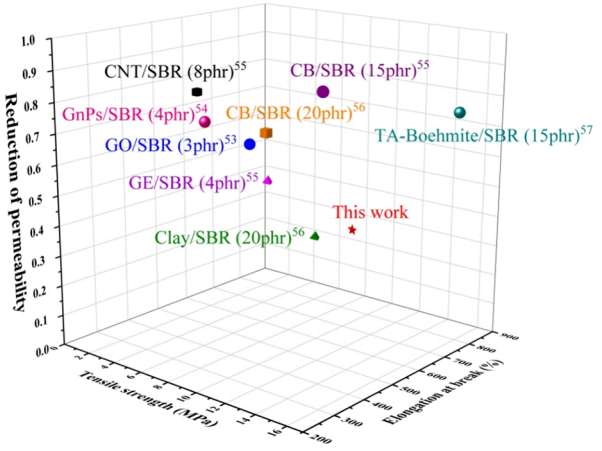

Figure 11. Comparison of tensile strength, elongation at break, and reduction in permeability of the composites between this work and other previously published works. Data in the bracket is the filler content.

4. CONCLUSIONS

In this work, GO@LDHs hybrids were prepared through the electrostatic self-assembly method, and the GO/LDHs mass ratio was found to affect the morphological microstructure of the hybrids. When the GO/LDHs was 1/3, GO and LDHs formed an interpenetrating isolated dispersion structure, with LDHs effectively preventing the aggregation of GO. Furthermore, the metal cations on LDHs formed an interlayer interaction with hydroxyl groups on GO basal planes and bridging bonding with carboxylic acid groups at the edge of GO sheets. Subsequently, the obtained GO@LDHs hybrids were compounded with SBR through a latex compounding process, resulting in uniform dispersion of GO@LDHs hybrids within the SBR matrix and the formation of a strong interaction with the SBR matrix, endowing the SBR composite with excellent comprehensive performance. Specifically, GO@LDHs/SBR composites showed remarkable tensile strength, high elongation at the break, and gas barrier properties. Compared with pure SBR, the N_2 gas permeability of GO@LDHs/SBR composites decreased by 52.2%, while the fracture toughness increased by 845%. In conclusion, the development of GO@LDHs hybrids provides promising prospects for the design of rubber composites with an enhanced gas barrier and mechanical properties.

AUTHOR INFORMATION

Corresponding Authors

Long Zheng − *Hubei Key Laboratory for New Textile Materials and Applications, College of Materials Science and Engineering, Wuhan Textile University, Wuhan 430020, China;* orcid.org/0009-0005-2134-8828; Email: lzheng@wtu.edu.cn

Shipeng Wen − *State Key Laboratory of Organic−Inorganic Composites, Beijing University of Chemical Technology, Beijing 100029, China;* orcid.org/0000-0001-9540-1314; Email: wensp@mail.buct.edu.cn

Authors

Xi Zhang − *College of Light Industry Science and Engineering, Beijing Technology and Business University, Beijing 100048, China*

Zongchao Xu − *State Key Laboratory of Organic−Inorganic Composites, Beijing University of Chemical Technology, Beijing 100029, China*

Chongzhi Sun − *State Key Laboratory of Organic−Inorganic Composites, Beijing University of Chemical Technology, Beijing 100029, China*

Complete contact information is available at: https://pubs.acs.org/10.1021/acsomega.4c05304

Notes

The authors declare no competing financial interest.

ACKNOWLEDGMENTS

The authors acknowledge the financial support from the National Natural Science Foundation of China, China (52273049, 52303063, and 52003017).

REFERENCES

(1) Guo, B.; Tang, Z.; Zhang, L. Transport performance in novel elastomer nanocomposites: Mechanism, design and control. *Prog. Polym. Sci.* **2016**, *61*, 29−66.

(2) Zheng, L.; Jerrams, S.; Xu, Z.; Zhang, L.; Liu, L.; Wen, S. Enhanced gas barrier properties of graphene oxide/rubber composites with strong interfaces constructed by graphene oxide and sulfur. *Chemical Engineering Journal* **2020**, *383*, No. 123100.

(3) Mehta, I. P.; Pande, S. N.; Patel, M. B.; Virdi, G. T. Effect of Tire Inflation Pressure on Rolling Resistance, Contact Patch Area and Braking Distance. *Int. J. Sci. Technol. Eng.* **2017**, *3* (10), 384−388.

(4) Waddell, W. H.; Napier, R. C.; Evans, L. R.; Popio, J. A.; Douglas, R.; Rajapakshe, M. How tread loss affects rolling resistance. *Rubber Plast. News* **2014**, 14−18.

(5) Zhang, C.; An, X.; Tang, Z.; Fang, S.; Guo, B.; Zhang, L.; Liu, F.; Liu, J.; Chen, Z. Creation of Tortuosity in Unfilled Rubber via Heterogeneous Cross-Linking toward Improved Barrier Property. *Macromolecules* **2021**, *54* (24), 11522−11532.

(6) Wang, L.; Dou, Y.; Wang, J.; Han, J.; Liu, L.; Wei, M. Layer-by-layer assembly of layered double hydroxide/rubber multilayer films with excellent gas barrier property. *Composites Part A: Applied Science and Manufacturing* **2017**, *102*, 314−321.

(7) Wu, Y.-P.; Wang, Y.-Q.; Zhang, H.-F.; Wang, Y.-Z.; Yu, D.-S.; Zhang, L.-Q.; Yang, J. Rubber-pristine clay nanocomposites prepared by co-coagulating rubber latex and clay aqueous suspension. *Compos. Sci. Technol.* **2005**, *65* (7), 1195−1202.

(8) Xing, W.; Tang, M.; Wu, J.; Huang, G.; Li, H.; Lei, Z.; Fu, X.; Li, H. Multifunctional properties of graphene/rubber nanocomposites fabricated by a modified latex compounding method. *Compos. Sci. Technol.* **2014**, *99*, 67−74.

(9) Kwon, O. S.; Lee, D.; Lee, S. P.; Kang, Y. G.; Kim, N. C.; Song, S. H. Enhancing the mechanical and thermal properties of boron nitride

nanoplatelets/elastomer nanocomposites by latex mixing. *RSC Adv.* **2016**, *6* (65), 59970−59975.
(10) Raef, M.; Razzaghi-Kashani, M. The role of interface in gas barrier properties of styrene butadiene rubber-reduced graphene oxide composites. *Polymer* **2019**, *182*, No. 121816.
(11) Zheng, L.; Wang, D.; Xu, Z.; Zhang, L.; Liu, L.; Wen, S. High barrier properties against sulfur mustard of graphene oxide/butyl rubber composites. *Compos. Sci. Technol.* **2019**, *170*, 141−147.
(12) Yang, S.; Wu, H.; Xiong, Y.; Guo, S. In-situ constructing hybrid cross-linked networks in brominated butyl rubber via amphiphilic graphene oxide cross-linkers: Retaining excellent gas barrier and mechanical properties after fatigue. *Composites Part B: Engineering* **2024**, *272*, No. 111224.
(13) Zhang, Y.; Kentish, S.; Scholes, C. A. Reducing ammonia permeance in poly(acrylonitrile-co-butadiene) (NBR)-based elastomers. *J. Appl. Polym. Sci.* **2023**, *140* (42), No. e54566.
(14) Wang, L.; Zhang, J.; Sun, Y.; Zhang, T.; Wang, L.; Wang, J.; Liang, Y.; Hao, M.; Fu, Q. Green preparation and enhanced gas barrier property of rubber nanocomposite film based on graphene oxide-induced chemical crosslinking. *Polymer* **2021**, *225*, No. 123756.
(15) Li, H.; Yang, L.; Weng, G.; Xing, W.; Wu, J.; Huang, G. Toughening rubbers with a hybrid filler network of graphene and carbon nanotubes. *Journal of Materials Chemistry A* **2015**, *3* (44), 22385−22392.
(16) Lin, Y.; Zeng, Z.; Zhu, J.; Chen, S.; Yuan, X.; Liu, L. Graphene nanosheets decorated with ZnO nanoparticles: facile synthesis and promising application for enhancing the mechanical and gas barrier properties of rubber nanocomposites. *RSC Adv.* **2015**, *5* (71), 57771−57780.
(17) Basu, D.; Das, A.; Stöckelhuber, K. W.; Wagenknecht, U.; Heinrich, G. Advances in layered double hydroxide (LDH)-based elastomer composites. *Prog. Polym. Sci.* **2014**, *39* (3), 594−626.
(18) Yu, J.; Ruengkajorn, K.; Crivoi, D.-G.; Chen, C.; Buffet, J.-C.; O'Hare, D. High gas barrier coating using non-toxic nanosheet dispersions for flexible food packaging film. *Nat. Commun.* **2019**, *10* (1), 2398.
(19) Dou, Y.; Xu, S.; Liu, X.; Han, J.; Yan, H.; Wei, M.; Evans, D. G.; Duan, X. Transparent, Flexible Films Based on Layered Double Hydroxide/Cellulose Acetate with Excellent Oxygen Barrier Property. *Adv. Funct. Mater.* **2014**, *24* (4), 514−521.
(20) Yang, Z.; Shi, K.; Jin, Z.; Liu, Z.; Li, Y.; Huang, Y.; Gao, F.; Han, J. Biodegradable Layered Double Hydroxide/Polymer Films for Efficient Oxygen and Water Vapor Barriers. *Ind. Eng. Chem. Res.* **2022**, *61* (3), 1367−1374.
(21) Dou, Y.; Pan, T.; Xu, S.; Yan, H.; Han, J.; Wei, M.; Evans, D. G.; Duan, X. J. A. C. Transparent, ultrahigh-gas-barrier films with a brick-mortar-sand structure. *Angew. Chem.* **2015**, *127* (33), 9809−9814.
(22) Yang, Z.; Li, B.; Li, S.; Dou, Y.; Han, J. Layered double hydroxide/PBAT hybrid films with simultaneously high-barrier and degradable properties. *Chem. Eng. Sci.* **2023**, *280*, No. 119016.
(23) Li, D.; Lin, Q.; Liu, L.; Song, X.; Wang, Z.; Sun, X.; Xue, Y.; Fu, Y.; Shi, Y.; Li, Z.; et al. Intercalation of silsesquioxane surfactant in layered double hydroxide for silicone rubber composites: Enhancing interfacial interactions toward improvement of mechanical, thermal, and gas barrier properties. *Polym. Compos.* **2023**, *44* (12), 8389−8402.
(24) Hummers, W. S.; Offeman, R. E. Preparation of graphitic oxide. *J. Am. Chem. Soc.* **1958**, *80* (6), 1339−1339.
(25) Zhao, Y.; Li, F.; Zhang, R.; Evans, D. G.; Duan, X. Preparation of Layered Double-Hydroxide Nanomaterials with a Uniform Crystallite Size Using a New Method Involving Separate Nucleation and Aging Steps. *Chem. Mater.* **2002**, *14* (10), 4286−4291.
(26) Bhattacharya, M.; Bhowmick, A. K. Polymer-filler interaction in nanocomposites: New interface area function to investigate swelling behavior and Young's modulus. *Polymer* **2008**, *49* (22), 4808−4818.
(27) Xu, Z.; Gao, C. Aqueous Liquid Crystals of Graphene Oxide. *ACS Nano* **2011**, *5* (4), 2908−2915.
(28) Konkena, B.; Vasudevan, S. Understanding Aqueous Dispersibility of Graphene Oxide and Reduced Graphene Oxide through pKa Measurements. *J. Phys. Chem. Lett.* **2012**, *3* (7), 867−872.
(29) Mao, Y.; Wen, S.; Chen, Y.; Zhang, F.; Panine, P.; Chan, T. W.; Zhang, L.; Liang, Y.; Liu, L. High Performance Graphene Oxide Based Rubber Composites. *Sci. Rep.* **2013**, *3* (1), 2508.
(30) Evans, D. G.; Duan, X. Preparation of layered double hydroxides and their applications as additives in polymers, as precursors to magnetic materials and in biology and medicine. *Chem. Commun.* **2006**, *5*, 485−496.
(31) Saleem, H.; Haneef, M.; Abbasi, H. Y. Synthesis route of reduced graphene oxide via thermal reduction of chemically exfoliated graphene oxide. *Mater. Chem. Phys.* **2018**, *204*, 1−7.
(32) Toh, S. Y.; Loh, K. S.; Kamarudin, S. K.; Daud, W. R. W. Graphene production via electrochemical reduction of graphene oxide: Synthesis and characterisation. *Chemical Engineering Journal* **2014**, *251*, 422−434.
(33) Guo, H.-L.; Wang, X.-F.; Qian, Q.-Y.; Wang, F.-B.; Xia, X.-H. A Green Approach to the Synthesis of Graphene Nanosheets. *ACS Nano* **2009**, *3* (9), 2653−2659.
(34) Li, G.; Zhang, P.; Huo, S.; Fu, Y.; Chen, L.; Wu, Y.; Zhang, Y.; Chen, M.; Zhao, X.; Song, P. Mechanically Strong, Thermally Healable, and Recyclable Epoxy Vitrimers Enabled by ZnAl-Layer Double Hydroxides. *ACS Sustainable Chem. Eng.* **2021**, *9* (6), 2580−2590.
(35) Hatami, H.; Fotovat, A.; Halajnia, A. Comparison of adsorption and desorption of phosphate on synthesized Zn-Al LDH by two methods in a simulated soil solution. *Appl. Clay Sci.* **2018**, *152*, 333−341.
(36) Zhang, B.; Hu, R.; Sun, D.; Wu, T.; Li, Y. Fabrication of Magnetite-Graphene Oxide/MgAl-Layered Double Hydroxide Composites for Efficient Removal of Emulsified Oils from Various Oil-in-Water Emulsions. *J. Chem. Eng. Data* **2018**, *63* (12), 4689−4702.
(37) Park, S.; Lee, K.-S.; Bozoklu, G.; Cai, W.; Nguyen, S. T.; Ruoff, R. S. Graphene Oxide Papers Modified by Divalent Ions-Enhancing Mechanical Properties via Chemical Cross-Linking. *ACS Nano* **2008**, *2* (3), 572−578.
(38) Ching, K.; Lian, B.; Leslie, G.; Chen, X.; Zhao, C. Metal-cation-modified graphene oxide membranes for water permeation. *Carbon* **2020**, *170*, 646−657.
(39) Lin, X.; Shen, X.; Sun, X.; Liu, X.; Wu, Y.; Wang, Z.; Kim, J.-K. Graphene Oxide Papers Simultaneously Doped with Mg^{2+} and Cl^{-} for Exceptional Mechanical, Electrical, and Dielectric Properties. *ACS Appl. Mater. Interfaces* **2016**, *8* (3), 2360−2371.
(40) Xu, Z.; Zheng, L.; Wen, S.; Liu, L. Graphene oxide-supported zinc oxide nanoparticles for chloroprene rubber with improved crosslinking network and mechanical properties. *Composites Part A: Applied Science and Manufacturing* **2019**, *124*, No. 105492.
(41) Wang, G.; Rao, D.; Li, K.; Lin, Y. UV Blocking by Mg-Zn-Al Layered Double Hydroxides for the Protection of Asphalt Road Surfaces. *Ind. Eng. Chem. Res.* **2014**, *53* (11), 4165−4172.
(42) Stankovich, S.; Dikin, D. A.; Piner, R. D.; Kohlhaas, K. A.; Kleinhammes, A.; Jia, Y.; Wu, Y.; Nguyen, S. T.; Ruoff, R. S. Synthesis of graphene-based nanosheets via chemical reduction of exfoliated graphite oxide. *Carbon* **2007**, *45* (7), 1558−1565.
(43) Rastin, H.; Saeb, M. R.; Nonahal, M.; Shabanian, M.; Vahabi, H.; Formela, K.; Gabrion, X.; Seidi, F.; Zarrintaj, P.; Sari, M. G.; et al. Transparent nanocomposite coatings based on epoxy and layered double hydroxide: Nonisothermal cure kinetics and viscoelastic behavior assessments. *Prog. Org. Coat.* **2017**, *113*, 126−135.
(44) Amirov, R. R.; Shayimova, J.; Nasirova, Z.; Dimiev, A. M. Chemistry of graphene oxide. Reactions with transition metal cations. *Carbon* **2017**, *116*, 356−365.
(45) Tang, Z.; Wu, X.; Guo, B.; Zhang, L.; Jia, D. Preparation of butadiene-styrene-vinyl pyridine rubber-graphene oxide hybrids through co-coagulation process and in situ interface tailoring. *J. Mater. Chem.* **2012**, *22* (15), 7492−7501.
(46) Scherillo, G.; Lavorgna, M.; Buonocore, G. G.; Zhan, Y. H.; Xia, H. S.; Mensitieri, G.; Ambrosio, L. Tailoring Assembly of Reduced Graphene Oxide Nanosheets to Control Gas Barrier Properties of Natural Rubber Nanocomposites. *ACS Appl. Mater. Interfaces* **2014**, *6* (4), 2230−2234.

https://doi.org/10.1021/acsomega.4c05304
ACS Omega 2024, 9, 39846−39855

(47) Barick, A. K.; Tripathy, D. K. Effect of organically modified layered silicate nanoclay on the dynamic viscoelastic properties of thermoplastic polyurethane nanocomposites. *Appl. Clay Sci.* **2011**, *52* (3), 312−321.
(48) Xu, Z.; Song, Y.; Zheng, Q. Payne effect of carbon black filled natural rubber compounds and their carbon black gels. *Polymer* **2019**, *185*, No. 121953.
(49) Liu, X.; Kuang, W.; Guo, B. Preparation of rubber/graphene oxide composites with in-situ interfacial design. *Polymer* **2015**, *56*, 553−562.
(50) Lin, Y.; Liu, S.; Peng, J.; Liu, L. The filler-rubber interface and reinforcement in styrene butadiene rubber composites with graphene/silica hybrids: A quantitative correlation with the constrained region. *Composites Part A: Applied Science and Manufacturing* **2016**, *86*, 19−30.
(51) Zhang, X.; Loo, L. S. Study of Glass Transition and Reinforcement Mechanism in Polymer/Layered Silicate Nanocomposites. *Macromolecules* **2009**, *42* (14), 5196−5207.
(52) Wang, Z. F.; Wang, B.; Qi, N.; Zhang, H. F.; Zhang, L. Q. Influence of fillers on free volume and gas barrier properties in styrene-butadiene rubber studied by positrons. *Polymer* **2005**, *46* (3), 719−724.
(53) Zheng, L.; Jerrams, S.; Su, T.; Xu, Z.; Zhang, L.; Liu, L.; Wen, S. Enhanced covalent interface, crosslinked network and gas barrier property of functionalized graphene oxide/styrene-butadiene rubber composites triggered by thiol-ene click reaction. *Composites Part B: Engineering* **2020**, *197*, No. 108186.
(54) Gaca, M.; Vaulot, C.; Maciejewska, M.; Lipińska, M. Preparation and Properties of SBR Composites Containing Graphene Nanoplatelets Modified with Pyridinium Derivative. *Materials* **2020**, *13* (23), 5407.
(55) Wen, S.; Zhang, R.; Xu, Z.; Zheng, L.; Liu, L. Effect of the Topology of Carbon-Based Nanofillers on the Filler Networks and Gas Barrier Properties of Rubber Composites. *Materials* **2020**, *13* (23), 5416.
(56) Wang, Y.; Zhang, H.; Wu, Y.; Yang, J.; Zhang, L. Preparation, structure, and properties of a novel rectorite/styrene-butadiene copolymer nanocomposite. *J. Appl. Polym. Sci.* **2005**, *96* (2), 324−328.
(57) Tang, Z.; Zhang, C.; Zhu, L.; Guo, B. Low permeability styrene butadiene rubber/boehmite nanocomposites modified with tannic acid. *Materials & Design* **2016**, *103*, 25−31.

https://doi.org/10.1021/acsomega.4c05304
ACS Omega 2024, 9, 39846−39855